ELSEVIER

15 May 1997

OPTICS COMMUNICATIONS

Optics Communications 138 (1997) 158–171

Full length article

Classical and quantum properties of the subharmonic-pumped parametric oscillator

Stephan Schiller [1], Robert Bruckmeier, Andrew G. White [2]

Fakultät für Physik, Universität Konstanz, D-78434 Konstanz, Germany

Received 7 September 1996; accepted 19 December 1996

Abstract

A model for nondegenerate optical parametric oscillation in a continuous-wave singly resonant frequency doubler is presented. General expressions for the stationary state properties, such as threshold and conversion efficiency are derived for arbitrary focusing and arbitrary second-harmonic generation as well as parametric generation wavevector mismatches $\Delta k, \Delta K$. For large Δk, where the SHG efficiency decreases roughly as $|\Delta k|^{-2}$, the oscillation threshold increases roughly linearly with $|\Delta k|$. Substantial conversion efficiencies for the generation of signal and idler powers are predicted for cavities with good escape efficiency. Further salient features are optical limiting of the harmonic output at zero wavevector mismatches and parametric generation-induced second-harmonic generation when $\Delta kL = 2\pi N$. The quantum properties of the system are a special case of the doubly-resonant frequency doubler discussed by Marte [Phys. Rev. Lett. 74 (1995) 4815]: the system is predicted to be a source of highly quantum correlated signal and idler waves (twin beams).

PACS: 42.65.Ky
Keywords: Harmonic generation; Frequency conversion

1. Introduction and overview

Externally resonant frequency conversion plays an increasingly important role in extending the spectral range of single-frequency continuous-wave lasers, as well as for the generation of nonclassical states of light and quantum measurements. Of the nonlinear optical processes used, the simplest one is singly-resonant second-harmonic generation (SHG), in which a subharmonic wave (ω_1) is resonantly enhanced in an optical cavity (Fig. 1) [1]. The resulting high circulating power leads to high external conversion efficiency for the generation of a harmonic wave ($2\omega_1$); values as high as 89% have been reached [2–4]. A frequency doubler also represents a simple and reliable source of bright squeezed light: the harmonic wave generated through singly-resonant SHG is squeezed in the amplitude quantum noise [5–7].

The apparently simple process of singly-resonant SHG is surprisingly rich in possible effects and the present paper is devoted to a detailed discussion of some of them. As an overview, Fig. 2 shows a phase diagram of some possible behavior of a plane-wave resonant frequency doubler as a function of the two parameters usually under control of the experimenter, the subharmonic input power and the SHG wavevector mismatch $\Delta k = k(2\omega_1) - 2k(\omega_1)$. For the standard use as a harmonic generator, the characteristic input power scale is P^*, where, for fixed input mirror transmission, the conversion

[1] http://quantum-optics.physik.uni-konstanz.de; E-mail: stephan.schiller@uni-konstanz.de.
[2] Present address: Department of Physics, Australian National University, Canberra ACT 0200, Australia.

PII S0030-4018(96)00793-6

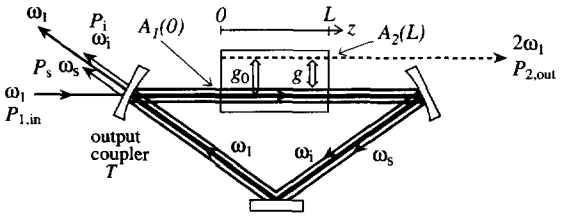

Fig. 1. Schematic of a subharmonic pumped parametric oscillator (SPO). A resonant subharmonic wave (full line) generates a harmonic wave ($2\omega_1$, dashed) which in turn generates resonant signal ω_s and idler ω_i waves (dashed). The harmonic wave is not resonant. The four waves are shown not overlapping for clarity.

efficiency is maximum [3]. P^* scales as $\mathrm{sinc}^{-2}(\Delta kL/2)$, being minimum at zero wavevector mismatch, the preferred operation point.

If at $\Delta kL = 0$ the input power is increased beyond P^* (with the input mirror transmission still fixed), the nonresonant harmonic field generated in the nonlinear medium is large enough to provide a gain for a nondegenerate signal/idler mode pair. If it exceeds their cavity losses parametric oscillation can set in. This process is termed subharmonic-pumped parametric oscillation (SPO) since it converts photons of frequency ω_1 to photons of frequencies ω_s and ω_i through the intermediary of the harmonic wave $2\omega_1$. Subharmonic-pumped parametric oscillation in singly-resonant SHG was first observed in a monolithic $MgO:LiNbO_3$ resonator pumped by a Nd:YAG laser [8,9]. Subsequently, a tunable, frequency-stable and efficient SPO has been demonstrated using a semi-monolithic resonator [10]. Recently, also the quantum properties of the harmonic wave in the SPO regime have been studied [11]. SPO can also occur in *doubly-resonant* frequency doublers, with a much smaller threshold, and has been demonstrated earlier [12].

The threshold power for SPO is an important issue. With increasing $|\Delta k|$ one expects an increasing threshold, since the generated harmonic power decreases. This indeed occurs in the limit of large $|\Delta kL|$, as shown in Fig. 2. However, there is no direct connection between SHG efficiency and SPO threshold. Indeed, a noteworthy feature appears: the occurrence of SPO even at values where the *external* SHG efficiency vanishes ($\Delta kL = 2\pi N$ for weak focusing). This is due to the presence of sufficient harmonic power *within* the nonlinear medium to drive the oscillation.

The domain of nonzero wavevector mismatch also harbors cascaded second-order nonlinear effects [13]. These lead to Kerr-like nonlinear phase shifts for the subharmonic wave, which may develop into optical bistability [14]. The corresponding power scale, calculated under the assumption that SPO is suppressed in some way (for example, due to large signal and idler detunings, or signal and idler cavity losses sufficiently higher than the subharmonic loss) is shown in Fig. 2. The nonlinear phase shifts are also relevant below this power scale and must be considered in determining the properties of SPO.

In this paper we present a theoretical model for the SPO (Section 2) which complements the discussion of some basic characteristics of the SPO given earlier [9]. In Section 3, we provide expressions for the threshold power and the conversion efficiency, taking into account focusing of the resonator modes, wavevector mismatch of both the second-harmonic and parametric generation processes and thus nonlinear phase shift effects. A theoretical overview of the quantum properties of the device is presented in Section 4, with the purpose of evaluating effects of SPO on the quantum noise reduction studied in recent SHG experiments [5–7,11] and to verify the ability of SPO to serve as a source of quantum correlated waves (twin beams) [15].

2. Classical description of SPO

2.1. The system

Fig. 1 shows a schematic of the nonlinear system to be discussed in this work. The input subharmonic wave is injected into a cavity where it generates a nonresonant harmonic wave. The latter can act as a pump wave for nondegenerate oscillation (signal and idler frequencies $\omega_{s/i} \neq \omega_1$) if its average power along the crystal length is high enough.

The important physical distinction between SPO and usual OPO is that even at threshold the pump ($2\omega_1$) wave amplitude is not constant along the nonlinear medium, but spatially dependent, because it is generated internally from the circulating

[3] Note that maximization of conversion efficiency via input coupler transmission at fixed input power yields a different result as compared to the maximization via input power at fixed input coupler transmission.

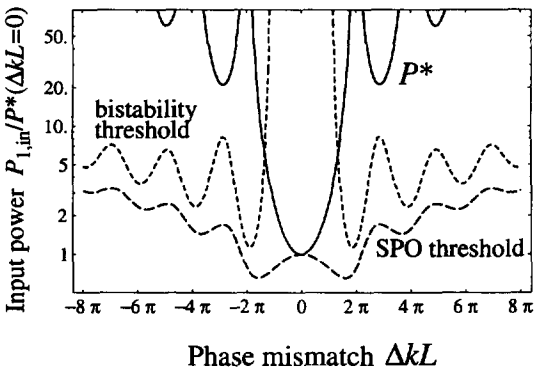

Fig. 2. Phase diagram for externally resonant SHG. The SPO threshold power is $P^{\text{th}}_{1,\text{in}}(\Delta kL,\Delta K=0)$. $P^*(\Delta k)$ is the input (ω_1) power at which the SHG conversion efficiency is maximum. The threshold for optical bistability due to cascaded second-order nonlinearity is calculated using Ref. [14]

fundamental wave. The spatial dependence of the pump wave is therefore a function of the SHG wavevector mismatch Δk. This is one ingredient that will be taken into account in the calculations below. We also consider an arbitrary wavevector mismatch $\Delta K = k(2\omega) - k(\omega_i) - k(\omega_s)$ for the nondegenerate parametric process. The inclusion of both Δk and Δk effects allows the derivation of important properties of the SPO, such as the temperature dependence of its threshold and output wavelengths.

A quantitative description of the SPO requires the evolution equations of the amplitudes of the electric fields within the nonlinear medium. Since, to our knowledge, equations that take into account arbitrary focusing of the modes do not appear to be widely known or used, we present here an explicit derivation.

2.2. Derivation of equations of propagation for general focusing

In this section we solve Maxwell's equations for wave propagation in the presence of a nonlinear polarization P_{NL}. Walk-off effects are not considered. A wave of frequency ω whose electric field E is along the direction of an index axis satisfies the wave equation

$$\left(\partial_z^2 + \partial_x^2 + \partial_y^2\right)E - \frac{n^2}{c^2}\ddot{E} = \mu_0 \ddot{P}_{\text{NL}}\,, \tag{1}$$

where P_{NL} is the contribution to the nonlinear polarization oscillating at the same frequency as E, n is the index of refraction at the frequency ω, c is the speed of light in vacuum, and μ_0 is the vacuum magnetic permeability. Let the propagation direction be along positive z, z_0 being the position of the focus (not necessarily within the nonlinear medium). We express the fields as

$$E = \text{Re}\left(e^{-ikz+i\omega t}\tilde{E}(x,y,z)\right), \qquad P_{\text{NL}} = \text{Re}\left(e^{-ikz+i\omega t}\tilde{P}_{\text{NL}}(x,y,z)\right), \tag{2}$$

with the envelopes $\tilde{E}$, $\tilde{P}_{\text{NL}}$ and $k = n\omega/c$. Applying the slowly varying envelope approximation, $|\partial_z^2 \tilde{E}| \ll k\,|\partial_z \tilde{E}|$, we obtain the paraxial equation

$$\left(\partial_z + \frac{i}{2k}\left(\partial_x^2 + \partial_y^2\right)\right)\tilde{E} = -\frac{i\omega\mu_0 c}{2n}\tilde{P}_{\text{NL}}\,. \tag{3}$$

The electric field envelope is now expanded in terms of the complete set of orthonormal cylindrical TEM_{mn} modes ψ_{mn} [18],

$$\tilde{E}(x,y,z) = \sqrt{\frac{\omega}{n}}\sum_{mn} A_{mn}(z)\,\psi_{mn}(x,y,z)\,, \tag{4}$$

where the basis modes with waist parameter w and beam waist position z_0 are solutions of the source-free equation

$$\left(\partial_z + \frac{i}{2k}\left(\partial_x^2 + \partial_y^2\right)\right)\psi_{mn} = 0\,. \tag{5}$$

Note that the above expansion uses a z-dependent basis. The mode expansion coefficients are

$$A_{mn}(z) = \sqrt{n/\omega} \int \tilde{E} \psi_{mn}^* \, \mathrm{d}x \, \mathrm{d}y \tag{6}$$

and depend on z only. The optical power in a mode is given by $\omega |A_{mn}|^2 / 2c\mu_0$, so $|A_{mn}|^2$ is scaled to be proportional to the photon number rate.

The paraxial equation (3) can be solved by introducing the Green function [16,17]

$$G(x,y,z) = \frac{ik}{2\pi z} \exp\left(-\frac{ik}{2z}(x^2 + y^2) \right) \Theta(z), \tag{7}$$

where $\Theta(z)$ is the step function. G satisfies the wave equation

$$\left(\partial_z + \frac{i}{2k} \left(\partial_x^2 + \partial_y^2 \right) \right) G = \delta^3(\boldsymbol{x}). \tag{8}$$

With the help of G, the electric field generated by the nonlinear polarization is found as

$$\tilde{E}(\boldsymbol{x}) = -\frac{i\omega\mu_0 c}{2n} \int G(\boldsymbol{x} - \boldsymbol{x}') \tilde{P}_{\mathrm{NL}}(\boldsymbol{x}') \, \mathrm{d}^3 x'. \tag{9}$$

We now focus our attention on the expansion coefficients A_{mn} of the field. They satisfy the differential equation

$$\frac{\mathrm{d}A_{mn}(z)}{\mathrm{d}z} = -\frac{i\mu_0 c}{2} \sqrt{\frac{\omega}{n}} \int \tilde{P}_{\mathrm{NL}}(x,y,z) \, \psi_{mn}^*(x,y,z) \, \mathrm{d}x \, \mathrm{d}y. \tag{10}$$

This represents the important basic relation which will be specialized below. It can be derived by inserting Eq. (9) into Eq. (6), expressing ∂_z in terms of the paraxial operator $\partial_z + i(\partial_x^2 + \partial_y^2)/2k$, using Eqs. (5) and (8) and performing a partial integration of $\partial_x^2 + \partial_y^2$.

We turn now to the application of Eq. (10) to the SPO. The four waves of relevance here are taken to be the TEM_{00} modes, so we introduce the short-hand A for the coefficients A_{00}, labeled by 1, 2, s, i. j will be used as a general index. The focusing of the resonant waves (1,s,i) is defined by the geometry of the common resonator. Consequently, these waves have identical Rayleigh ranges $z_r = k_j w_j^2/2$, where w_j are the respective beam waist sizes entering the Gaussians ψ_{00}. Since the harmonic is generated from the subharmonic TEM_{00}, it has a waist $\sqrt{2}$ times smaller and thus also the same Rayleigh range z_r. The foci of all waves are also at the same location z_0.

Following Boyd and Kleinman [16], we introduce new variables for the frequencies and indices of refraction, $\omega_s = \omega_1(1+\eta)$, $\omega_i = \omega_1(1-\eta)$, $n_s = n_1(1+\zeta)$, $n_i = n_1(1-\zeta)$. In the following we first consider the interaction between signal, idler and the $2\omega_1$ sum frequency waves, which will then be specialized to degenerate interaction between fundamental and second harmonic.

The nonlinear polarizations for sum frequency generation (SFG) and parametric generation are

$$\tilde{P}_{\mathrm{NL},2} = \beta \epsilon_0 \, d \tilde{E}_s \, \tilde{E}_i \, \mathrm{e}^{i\Delta K z}, \qquad \tilde{P}_{\mathrm{NL},s/i} = 2\epsilon_0 \, d \tilde{E}_2 \, \tilde{E}_{i/s}^* \, \mathrm{e}^{-i\Delta K z}, \tag{11}$$

where d is the nonlinear coefficient and $\Delta K = k(2\omega_1) - k(\omega_s) - k(\omega_i)$ is the phase mismatch. From $\chi^{(2)}$ tensor summation, $\beta = 2$ or $\beta = 1$ for nondegenerate ($\omega_i, \omega_s \leftrightarrow 2\omega_1$) and for degenerate ($\omega_1 \leftrightarrow 2\omega_1$) operation, respectively. Performing the integration on the r.h.s of Eq. (10) we obtain

$$\frac{\mathrm{d}A_2(z)}{\mathrm{d}z} = -i\frac{\beta}{2} g(\eta,\zeta) \, u(\Delta K, z) \, A_s(z) \, A_i(z), \qquad \frac{\mathrm{d}A_{s/i}}{\mathrm{d}z} = -ig(\eta,\zeta) \, u^*(\Delta K, z) \, A_2(z) \, A_{i/s}^*(z), \tag{12}$$

$$g(\eta,\zeta) = \frac{d\omega_1^2}{n_1 \sqrt{c^3 \pi z_r}} \frac{1-\eta^2}{1+\eta\zeta}, \qquad u(\delta,z) = \frac{\mathrm{e}^{i\delta z}}{1 - i(z - z_0)/z_r}. \tag{13}$$

The function g represents the gain, while u results form the overlap integral of three ψ_{00} functions with different waists. It describes the influence of wavevector mismatch and focusing. When the waves are weakly focused (near-field case) $u(\delta,z)$ reduces to $\exp(i\delta z)$. We have assumed operation sufficiently close to phase matching $\Delta K \simeq 0$ so that the harmonic index may be approximated by $n_2 = n_1(1+\eta\zeta)$. It is interesting to note that for SFG there is only gain for the TEM_{00} sum frequency mode, whereas the parametric gain affects many modes: the modematch of the generated field to the TEM_{00} mode is 75% for degenerate operation; i.e. 25% of the gain is distributed among non-TEM_{00}-modes.

Eqs. (12) are specialized for degenerate interaction by substituting $\beta = 1$, $\eta = 0$, $\zeta = 0$, s $\to$ 1, i $\to$ 1. Note that a different phase mismatch $\Delta K \to \Delta k = k(2\omega_1) - 2k(\omega_1)$ results. For the following discussion, the notation is simplified by introducing the gain coefficients $g = g(\eta,\zeta)$, $g_0 = g(0,0)$.

Adding the effects of degenerate and nondegenerate nonlinear interaction, the following propagation equations for the SPO result:

$$\frac{\mathrm{d}A_1(z)}{\mathrm{d}z} = -ig_0 u^*(\Delta k,z)\, A_1^*(z)\, A_2(z),$$

$$\frac{\mathrm{d}A_2(z)}{\mathrm{d}z} = -i\frac{g_0}{2}u(\Delta k,z)\, A_1(z)^2 - igu(\Delta K,z)A_i(z)A_s(z), \tag{14}$$

$$\frac{\mathrm{d}A_{i/s}(z)}{\mathrm{d}z} = -igu^*(\Delta K,z)\, A_{s/i}^*(z)\, A_2(z). \tag{15}$$

In this work we will find that the most relevant situation is near-degenerate operation, where $g \approx g_0$. We shall however keep the distinction between the two gain coefficients (i) to be able to identify quickly the interaction that leads to a particular coupling term in the equations of motion of the fields (see below) and (ii) because Eqs. (14) and (15) in this general form can be applied also to nonlinear media (notably quasi-phasematched materials) where even for near-degenerate interactions the $\omega_1 \leftrightarrow 2\omega_1$ and $\omega_i, \omega_s \leftrightarrow 2\omega_1$ gains are distinct due to distinct nonlinear coefficients d.

With minor changes in notation [4], special cases of Eqs. (14) and (15) have been employed to describe cascaded $\chi^{(2)}$ effects in wavevector-mismatched SHG [14] and doubly-resonant parametric oscillation [19].

2.3. Field propagation in the SPO

With the nonlinear medium enclosed in a high-finesse cavity, the amplitudes of signal, idler, and subharmonic will be nearly constant along the medium. We can therefore solve the propagation equations (14) and (15) in the mean field approximation by iterative integration to second order in the nonlinearities g_0 and g, similar to the approach by Lugiato et al. [20]. We start by integrating the equation for the harmonic wave,

$$A_2(L) - A_2(0) = -i\left(\frac{g_0 L}{2}\right) I(\Delta k)\, A_1(0)^2 - igLI(\Delta K)\, A_s(0)\, A_i(0). \tag{16}$$

$A_2(0)$ is the harmonic amplitude present at the input of the nonlinear medium. It is zero for the SPO but is considered here in view of the discussion of the quantum properties of the SPO. The coupling function I is defined by

$$I(\delta) = \int_0^L u(\delta,z)\,\mathrm{d}z/L. \tag{17}$$

We insert the result (16) into the propagation equations for the fundamental and signal/idler waves and obtain,

$$A_1(L) - A_1(0) = -\frac{a_1 L}{2}A_1(0) - ig_0 LI^*(\Delta k)\, A_1^*(0)\, A_2(0) - \left(\frac{g_0 gL^2}{2}\right) C(\Delta k,\Delta K)\, A_1(0)^*\, A_s(0)\, A_i(0) - \left(\frac{g_0^2 L^2}{4}\right) D(\Delta k)|A_1(0)|^2\, A_1(0), \tag{18}$$

$$A_{s/i}(L) - A_{s/i}(0) = -\frac{a_{s/i} L}{2}A_{s/i}(0) - igLI(\Delta K)^*\, A_{i/s}(0)^*\, A_2(0) - \left(\frac{g_0 gL^2}{4}\right) C(\Delta k,\Delta K)\, A_{i/s}(0)^*\, A_1(0)^2 - \left(\frac{g^2 L^2}{2}\right) D(\Delta K)|A_{i/s}(0)|^2\, A_{s/i}(0). \tag{19}$$

In these equations we have added the effect of propagation losses (power loss coefficients $a_{1/i/s}$ with $aL \ll 1$). By assumption, the right hand sides of Eqs. (18) and (19) are small. There is no such restriction on the right hand side of Eq. (16), however. The dimensionless coupling functions appearing in Eqs. (18) and (19) are

$$C(\delta_1,\delta_2) = \frac{2}{L^2}\int_0^L\int_0^z u^*(\delta_1,z)u(\delta_2,z')\,\mathrm{d}z'\,\mathrm{d}z, \qquad D(\delta) = C(\delta,\delta). \tag{20}$$

[4] The amplitudes A_j in Ref. [14] are $\sqrt{2/\pi w_j^2}$ times the amplitudes A_j used here. This gives rise to a factor $1/2$ in the equation for $\mathrm{d}A_1/\mathrm{d}z$ in Eq. (1) of Ref. [14]. The cavity fields α used in Refs. [14,19] are based on this different normalization and thus differ from the fields α defined in this work. The functions K, D in Ref. [19] are denoted by $I(\Delta K)$ and $D(\Delta K)$, respectively, here. The functions B and A in Ref. [8] are denoted by $I(\Delta k)$ and $D(\Delta k)$ here. The functions I and K in Ref. [14] are denoted by $I(\Delta k)$ and $D(\Delta k)$ here.

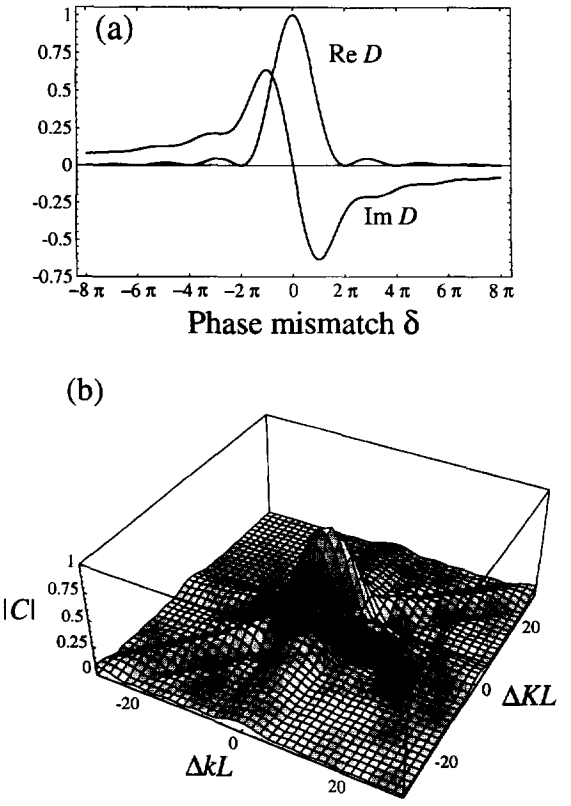

Fig. 3. (a) The self- and cross-interaction coupling function D. Plane-wave focusing assumed. (b) The parametric gain function C. The maximum is at $\Delta KL = \Delta kL$.

General relationships between these coupling functions can be easily derived by invoking overall energy conservation: the power balance between input powers at $z = 0$ and output powers at $z = L$ yields

$$\mathrm{Re}\, D(\delta) = |I(\delta)|^2, \qquad C(\delta_1,\delta_2) + C(\delta_2,\delta_1)^* = 2\, I(\delta_1)^*\, I(\delta_2). \tag{21}$$

For the special case of vanishing wavevector mismatches, $\Delta kL = \Delta kL = 0$, and plane-wave focusing, the coupling functions simply reduce to unity, $I = D = C = 1$.

What are the meanings of the coupling functions? $|I(\Delta k)|^2$ and $|I(\Delta K)|^2$ are the normalized nonlinear coefficients for SHG and sum frequency generation, respectively. For plane-wave focusing, these are the well-known $\mathrm{sinc}^2(\Delta kL/2)$ and $\mathrm{sinc}^2(\Delta KL/2)$ functions. For general focusing, $|I|^2$ is related to the familiar Boyd-Kleinman factor h by $|I|^2 = 2 z_r h/L$. $D(\Delta k)$ and $D(\Delta K)$ are the loss and self-phase shift coefficients due to harmonic and sum-frequency generation ($\omega_i + \omega_s \to 2\omega_1$), respectively. Fig. 3a is a plot of $D(\delta)$. The real part corresponds to the loss coefficient and the imaginary part to an effective Kerr phase shift coefficient, which occurs for nonzero phase mismatch.

$C(\Delta k,\Delta K)$ and $C(\Delta K,\Delta k)$ are the gain coefficients for subharmonic and parametric generation, respectively. The latter plays a central role for SPO. We can gain a qualitative understanding of the occurrence of SPO by considering the gain for signal and idler waves. From Eq. (15), we see that it is proportional to the spatially varying function $u^*(\Delta K,z)\, A_2(z)$. According to Eq. (14), the harmonic amplitude itself is given, below or at threshold, by $A_2(z) \sim \int_0^z u(\Delta k,z')\,\mathrm{d}z'$, since $A_1(z)$ is essentially constant. Thus, the gain coefficient integrated over the entire medium is just $L^2 C(\Delta K,\Delta k)$: it appears as the third term in Eq. (19). The crucial point is that C is nonzero for any wavevector mismatche. Fig. 3b shows the dependence of $|C(\Delta K,\Delta k)|$ on the two phase mismatches. $|C|$ exhibits relative maxima on the "ridges" $\Delta kL = 0$ and $\Delta KL = \Delta kL$ along which it decreases as $1/|\Delta kL|$ for large ΔkL. Below we will find that the SPO threshold has relative minima on these ridges.

The parametric gain is also proportional to the circulating subharmonic power A_1^2. It is known from the behaviour of a resonant frequency doubler that this power grows monotonically with input subharmonic power, independent of Δk (as long as $A_{i/s} = 0$). The gain will thus eventually exceed the loss of signal/idler and parametric oscillation will then set in. We conclude that the threshold for SPO is eventually reached for any value of wavevector mismatch.

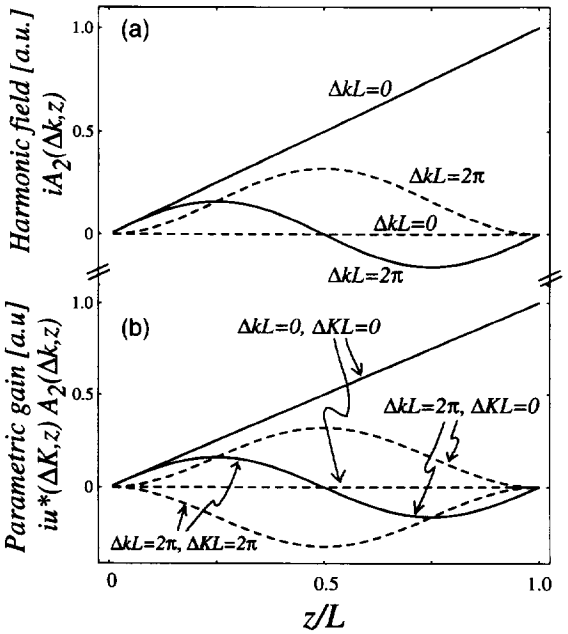

Fig. 4. Spatial dependence of (a) the harmonic field generated by SHG and (b) the ensuing parametric gain, for values of wavevector mismatches where $|C|$ is large. Full lines: real parts, dashed lines: imaginary parts.

As concrete examples, Figs. 4a and 4b show the harmonic field amplitude and the parametric gain coefficient, respectively, for three cases. Under perfect SHG phasematching, $\Delta k = 0$, the harmonic generation efficiency is maximum, A_2 grows linearly, and the average harmonic field in the crystal is one-half the output field. In the case of vanishing *external* harmonic conversion efficiency, e.g. at $\Delta kL = 2\pi$, the harmonic amplitude first grows and then is converted back to the fundamental wave, resulting in zero harmonic output at the end of the medium $A_2(L) = 0$. However, in both cases $A_2(z)$ is nonzero within the crystal. The spatial dependence of the gain coefficient, Fig. 4b leads to a finite magnitude for the average gain. The crucial observation here is that there is no direct connection between the harmonic amplitude at the end of the medium $A_2(L)$, which determines the emitted harmonic power, and the total parametric gain. This is the reason for occurrence of SPO even for vanishing external SHG efficiency.

3. The cavity equations

The description of the fields within the cavity is given in terms of equations of motion. To obtain them, the approximate solution for the propagation through the medium is complemented with the propagation through the remainder of the cavity. Selfconsistency relations are then imposed for the signal, idler and subharmonic fields at the input mirror of amplitude reflectivity r (equal for the three resonanting waves), whereby the high finesse limit $r \approx 1$ is taken [21]. We introduce the intracavity fields $\alpha_{1/i/s} = \sqrt{2\tau}\, A_{1/i/s}(0)$, where τ is the round-trip time of the cavity. Output and input fields $\alpha_{1/i/s,in/out}$ are equal to the respective amplitudes $\sqrt{2}\, A$. After eliminating the nonresonant harmonic wave we obtain the dynamical equations for the fields as

$$\dot{\alpha}_1 = -(\gamma + i\,\Delta_1)\alpha_1 - \sqrt{\mu\nu}\,C(\Delta k,\Delta K)\,\alpha_i\alpha_s\alpha_1^* - \frac{\mu}{2}D(\Delta k)\,|\alpha_1|^2\alpha_1 + \sqrt{2\gamma_c}\,\alpha_{1,in}\,,$$

$$\dot{\alpha}_{i/s} = -\left(\gamma + i\Delta_{i/s}\right)\alpha_{i/s} - \frac{\sqrt{\mu\nu}}{2}C(\Delta K,\Delta k)\,\alpha_1^2\alpha_{s/i}^* - \nu D(\Delta K)|\alpha_{s/i}|^2\alpha_{i/s}\,. \tag{22}$$

The input and output fields are related to the circulating fields by

$$\alpha_{1,in} + \alpha_{1,out} = \sqrt{2\gamma_c}\,\alpha_1\,, \quad \alpha_{i/s,out} = \sqrt{2\gamma_c}\,\alpha_{i/s}\,, \qquad \alpha_{2,out} = \sqrt{\mu}\,I(\Delta k)\alpha_1^2 + 2\sqrt{\nu}\,I(\Delta K)\,\alpha_i\alpha_s\,. \tag{23}$$

The harmonic field leaving the nonlinear medium has been defined as $\alpha_{2,out} = 2\,iA_2(L)$. The interaction strengths are $\mu = (g_0 L/2\tau)^2$ and $\nu = (gL/2\tau)^2$. $\Delta_{1/i/s}$ indicate detunings from the cavity resonance frequencies. The coupling and

decay rates (assumed equal for signal, idler and subharmonic) are defined as $\gamma_c = (1-r)/\tau$, $\gamma = \gamma_c + \gamma_l$, with $\gamma_l = (aL + b)/2\tau$ the sum of dissipation rates in the crystal and in the remainder of the cavity. The ratio γ_c/γ of the coupling to the total decay rate is the escape efficiency; it will be of relevance below. In terms of the input mirror transmission $T = 1 - r^2$ and the cavity round-trip loss $S = aL + b$, $\gamma_c/\gamma = T/(T+S)$.

In our nomenclature, the circulating powers are given by

$$P_{1/i/s} = \frac{\omega_{1/i/s}}{4c\mu_0}\frac{|\alpha_{1/i/s}|^2}{\tau}, \tag{24}$$

while the external powers are

$$P_{1,\mathrm{in/out}} = \frac{\omega_{1/i/s}}{4c\mu_0}|\alpha_{1,\mathrm{in/out}}|^2, \qquad P_{2,\mathrm{out}} = \frac{\omega_1}{4c\mu_0}|\alpha_{2,\mathrm{out}}|^2. \tag{25}$$

Note that the fields α are defined differently from the quantum optics convention; here $|\alpha_{1/i/s}|^2/\tau$, $|\alpha_{1,\mathrm{in/out}}|^2$, $|\alpha_{2,\mathrm{out}}|^2$ are not equal but proportional to photon fluxes.

3.1. Steady-state solution

The steady-state behavior of singly-resonant SHG and SPO is obtained from Eqs. (22) and (23) by setting the time derivatives to zero. The equations contain three free parameters, the detunings $\Delta_{1/i/s}$. The most relevant choice for Δ_1 is the one that maximizes the subharmonic power circulating in the cavity. This will maximize also the average harmonic amplitude and thus the parametric gain. With respect to signal/idler detuning $\Delta_{s/i}$, we are interested in those values that minimize the SPO threshold. Physically, this corresponds to allowing the SPO to "choose" a signal/idler mode pair with the lowest threshold. In practice, a pair exhibiting the optimum detunings may not exist. The minimum threshold calculated below is thus to be interpreted as the theoretical mimimum, which may be more or less close to experimentally observed threshold values. In performing the optimizations we must take into account that the coefficients C, D, may be complex. As can be seen from Eqs. (22), their nonvanishing imaginary parts give rise to intensity-dependent detunings. The contribution from $\mathrm{Im}\,D(\Delta k)$ and $\mathrm{Im}\,D(\Delta K)$, for example, represent effective Kerr self- and cross-couplings, respectively, due to "cascaded" second-order nonlinearity [8,22]. $\mathrm{Im}\,D(\Delta k)$ in particular leads to optical bistability as discussed in Section 1. To find the optimum detunings, we consider the magnitude squared of the second of Eqs. (22). Differentiating the expression implicitly with respect to $\Delta_{i/s}$, and setting $\mathrm{d}|\alpha_i|^2/\mathrm{d}\Delta = \mathrm{d}|\alpha_s|^2/\mathrm{d}\Delta = 0$, we obtain

$$\Delta_{s/i}^{\mathrm{opt}} + \nu\,\mathrm{Im}\,D(\Delta K)\,|\alpha_{i/s}|^2 = 0. \tag{26}$$

Thus, the cavity detunings are adjusted so that the nonlinear detunings are compensated. Assuming symmetry, $|\alpha_s|^2 = |\alpha_i|^2$, the simple relation

$$\gamma + \nu\,\mathrm{Re}\,D(\Delta K)\,|\alpha_{s/i}|^2 = \sqrt{\mu\nu}\,|C(\Delta K,\Delta k)||\alpha_1|^2 \tag{27}$$

is then found that expresses the circulating signal/idler power in terms of the circulating subharmonic power. Inserting this relation into the first of Eqs. (22), the subharmonic field α_1 may be eliminated, leaving an expression relating the circulating signal/idler power ($\sim|\alpha_{s/i}|^2$) to the input power ($\sim|\alpha_{1,\mathrm{in}}|^2$) only. Optimizing $|\alpha_{s/i}|^2$ again, now with respect to the subharmonic detuning Δ_1, yields the optimum value

$$\Delta_1^{\mathrm{opt}} = -\sqrt{\frac{\mu}{\nu}}\,\frac{\mathrm{Im}\,D(\Delta k)}{|C(\Delta K,\Delta k)|}\,\gamma - \frac{\sqrt{\mu\nu}}{2}\,\frac{\mathrm{Re}\,D(\Delta K)\,\mathrm{Im}\,D(\Delta k) - \mathrm{Im}(C(\Delta k,\Delta K)C(\Delta K,\Delta k))}{|C(\Delta K,\Delta k)|}|\alpha_{s/i}|^2. \tag{28}$$

The SPO threshold is found by inserting Eqs. (27) and (28) with $\alpha_i = 0$ into the first of Eqs. (22),

$$\frac{P_{1,\mathrm{in}}^{\mathrm{th}}}{\bar{P}} = \left(\frac{T+S}{T}\right)\frac{\left(|C(\Delta K,\Delta k)| + |I(\Delta k)|^2\right)^2}{|C(\Delta K,\Delta k)|^3}. \tag{29}$$

We have introduced the power scale $\bar{P} = (\omega_1/4c\mu_0)(\gamma^2/\nu)$. This power scale is independent of wavevector mismatch and depends on the material nonlinearity, the focusing of the modes and the resonator losses. To express $\bar{P}$ in terms of experimentally accessible parameters, we compare it with the threshold power P_{DRO} for doubly-resonant oscillation pumped by the harmonic wave. We find by a simple calculation

$$P_{\mathrm{DRO}} = \frac{\omega_1}{4c\mu_0}\,\frac{\gamma^2}{\nu|I(\Delta K)|^2} = \frac{\bar{P}}{|I(\Delta K)|^2} = \frac{(T+S)^2}{4\,E'_{\mathrm{NL}}}. \tag{30}$$

Here we have used the usual expression of the DRO threshold in terms of the conversion coefficient $E'_{NL} = L h \Gamma$, with the parametric nonlinearity $\Gamma = \mu_0 n_1 w_1^2 g^2$ and the Boyd-Kleinman factor h appropriate for the focusing and wavevector mismatch Δk at which the oscillator is operated. Near degeneracy, $\Gamma = 2\omega_1^3 d^2/\pi\epsilon_0 c^4 n_1^2$. In practice, E'_{NL} can be determined by measuring the efficiency of sum frequency generation $\omega_s + \omega_i \to 2\omega_1$. Using $|I|^2 = 2 z_r h/L$ we obtain

$$\bar{P} = \frac{z_r}{2L} \frac{(T+S)^2}{L\Gamma}. \tag{31}$$

A typical value for $\bar{P}$ in low-loss media, e.g. for parametric generation of 1064 nm in bulk $LiNbO_3$ ($\Gamma = 0.22/\mathrm{W\,m}$), is 10 mW.

Eqs. (29) and (31) permit the calculation of the theoretical minimum SPO threshold for any type of single-cavity SPO. The expressions are valid also for standing-wave cavities with double-pass of the harmonic (L is always the propagation distance in the nonlinear medium per round-trip) as long as relative phase shifts between the waves upon reflection at the back mirror are neglected.

The signal plus idler output power $P_s + P_i$ is given implicitly in terms of the "number of times above threshold", $P_{1.in}/P_{1.in}^{th}$, by

$$\frac{P_{1.in}}{P_{1.in}^{th}} = \left(1 + \frac{T+S}{4T}|I(\Delta K)|^2 \frac{P_s+P_i}{\bar{P}}\right)\left(1 + \frac{T+S}{4T}\xi\sqrt{\frac{\mu}{\nu}}\frac{P_s+P_i}{\bar{P}}\right)^2,$$

$$\xi = \frac{\left(|C(\Delta k,\Delta K)|^2 + |C(\Delta K,\Delta k)|^2\right)/2 - |I(\Delta k)I(\Delta K)|^2}{|C(\Delta K,\Delta k)| + \sqrt{\mu/\nu}\,|I(\Delta k)|^2}. \tag{32}$$

To obtain the harmonic output power one starts with the third of Eqs. (23) and finds

$$\frac{P_{2.out}}{\bar{P}} = \frac{4}{|C(\Delta K,\Delta k)|^2}\left|I(\Delta k) + \frac{T+S}{4T}\left[I(\Delta k)|I(\Delta K)|^2 - C(\Delta K,\Delta k)I(\Delta K)\right]\frac{P_s+P_i}{\bar{P}}\right|^2. \tag{33}$$

For completeness we also give the SHG conversion efficiency below threshold,

$$\frac{P_{2.out}}{P_{1.in}} = 2\frac{T}{T+S}\frac{\sqrt{|I(\Delta k)|^2 P_{2.out}/(\nu\bar{P}/\mu)}}{\left(1 + \frac{1}{2}\sqrt{|I(\Delta k)|^2 P_{2.out}/(\nu\bar{P}/\mu)}\right)^2}. \tag{34}$$

As is well known, for fixed mirror transmission, i.e. fixed escape efficiency, the SHG conversion efficiency exhibits a maximum value as a function of input power. This value is just the escape efficiency $T/(T+S)$ from the cavity, and is attained once the generated harmonic power reaches $P_{2.out} = 4\nu\bar{P}/\mu|I(\Delta k)|^2$. The corresponding input subharmonic power (plotted in Fig. 2) is

$$P^*(\Delta k) = \frac{4}{|I(\Delta k)|^2}\frac{T+S}{T}\frac{\nu}{\mu}\bar{P}. \tag{35}$$

We emphasize that all expressions given above, except for $\bar{P}$, depend on the phase mismatches.

The SPO threshold

Eq. (29) can be easily evaluated numerically for any focusing as determined by the cavity geometry of interest. Here we limit the discussion to the case of weak focusing, as well as $\mu = \nu$ in order to discuss the salient features. The most important result of Eq. (29) is that the threshold is always finite, since $|C(\Delta K,\Delta k)|$ never vanishes (Fig. 3a), although $I(\Delta k)$ does so at $\Delta kL = \pm 2\pi N$. Fig. 5 presents the inverse threshold of a plane-wave SPO as a function of both wavevector mismatches, calculated using Eq. (29). For comparison, Fig. 2 introduced in Section 1 is an excerpt in which ΔkL has been set to zero and only the SHG wavevector mismatch ΔkL is varied.

Low thresholds are attained when ΔkL is near 0 or ΔkL, due to the form of C. Along these branches, the SPO threshold increases approximately as $|\Delta kL|$ for large ΔkL. This increase, due to the decrease of the parametric gain $|C(\Delta K,\Delta k)| \sim 1/|\Delta kL|$, is related to the $1/|\Delta kL|$ dependence of the average harmonic field inside the nonlinear medium. It is important to note that this decrease is much weaker than the $|\Delta kL|^{-2}$ decrease of the SHG gain envelope ($|I(\Delta k)|^2$ in Fig. 4b). At any ΔkL, the minimum SPO threshold is equal on the two branches; this is a result specific to the near-field focusing geometry. A numerical evaluation for tight focusing shows that the near-degeneracy branch $\Delta KL = \Delta kL$ is slightly favored.

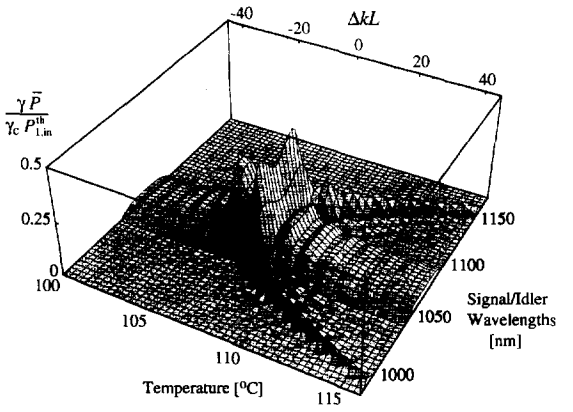

Fig. 5. The inverse SPO threshold for a $L = 1.5$ cm long plane-wave resonator of MgO:$LiNbO_3$ pumped by 1064 nm, as a function of crystal temperature T and output wavelengths. The hump at 1064 nm corresponds to $\Delta KL \simeq \Delta kL$, the parabolic hump corresponds to $\Delta KL \simeq 0$. The wavevector mismatch is $\Delta K = [7.5(T - 107°C)/K - 8.7 \times 10^3(1 - \omega_{1/s}/\omega_1)^2)\ cm^{-1}$.

At the special point $\Delta kL = \Delta KL = 0$ (hidden in Fig. 5) the SPO threshold is $P^{th}_{1,in}/\bar{P} = 4\gamma/\gamma_c = P^*(0)$, i.e. SPO threshold coincides with the input power at which the SHG efficiency is maximum [9]. This coincidence occurs more generally whenever $|C(\Delta K, \Delta k)| = |I(\Delta k)|^2$, Eqs. (29) and (35) then being equal, since $\mathrm{Re}\, D(\Delta k) = |I(\Delta k)|^2$. The SPO threshold is however not at a minimum at $\Delta kL = \Delta KL = 0$. The absolute minimum is taken on in the vicinity, with a significantly smaller value $P^{th}_{1,in}/\bar{P} = 2.08\,\gamma/\gamma_c$.

Optical limiting of the harmonic power

Fig. 6 presents the calculated conversion efficiencies for signal/idler generation, $(P_s + P_i)/P_{1,in} = 2\gamma_c(|\alpha_s|^2 + |\alpha_i|^2)/|\alpha_{1,in}|^2$ and for the emitted harmonic power, $P_{2,out}/P_{1,in} = |\alpha_{2,out}|^2/|\alpha_{1,in}|^2$.

For $\Delta k = \Delta K = 0$ the SHG conversion efficiency reaches the maximum value, equal to the escape efficiency, at threshold. Above threshold, the harmonic output power remains clamped at its value just below the onset of parametric oscillation since the second term in the absolute value in Eq. (33) vanishes. The harmonic power is fixed at $P_{2,out} = 4\bar{P} = \gamma_c P^{th}_{1,in}/\gamma$ so that the harmonic efficiency drops as $\gamma_c P^{th}_{1,in}/\gamma P_{1,in}$. The signal/idler output power on the other hand is a linear function of the input power, $P_s + P_i = (\gamma_c/\gamma)^2(P_{1,in} - P^{th}_{1,in})$, with a slope efficiency equal to the square of the escape efficiency.

This "optical limiter" effect has been discussed earlier for SPO in doubly-resonant SHG by Marte [23]; a similar effect has been studied by Siegman in standing-wave DROs more than 30 years ago [24]. Note that in the SPO the optical limiter effect appears more generally when $I(\Delta k)I(\Delta K)^* = C(\Delta K, \Delta k)$. Limiting in SPOs has recently been observed experimentally [11,10].

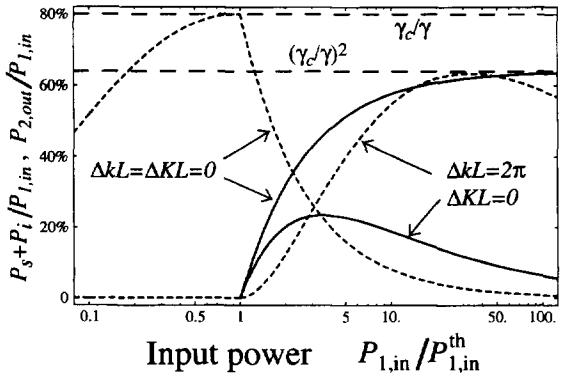

Fig. 6. Input-output power conversion efficiencies from subharmonic to signal/idler (full lines) and subharmonic to harmonic (dashed), as a function of subharmonic input power. Optical limiting $P_{2,out} = \text{const.}$ ($\Delta kL = \Delta KL = 0$) and SPO-induced SHG ($\Delta kL = 2\pi$, $\Delta KL = 0$) are shown. The cavity escape efficiency is chosen as $\gamma_c/\gamma = 0.8$.

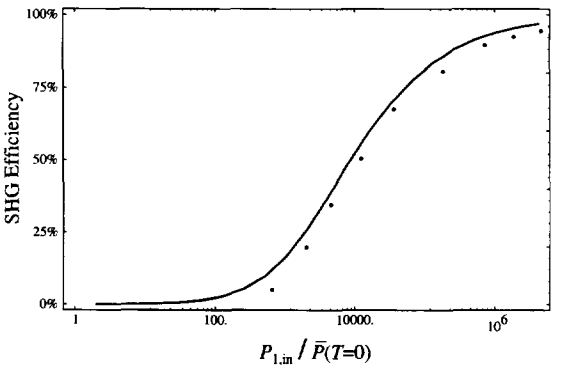

Fig. 7. Optimum SHG efficiency without SPO and for SPO at large SHG phase mismatch. The cavity escape efficiency is optimized at each input power level. Line: no SPO, $\Delta kL = 21\pi$. Points: SPO-induced SHG, $\Delta kL = 20\pi$. The parametric generation wavevector mismatch was set to $\Delta K = 0$, and $\nu = \mu$.

SPO-induced SHG

An interesting phenomenon occurs when the wavevector mismatch is such that $I(\Delta k) = 0 = \mathrm{Re}\, D(\Delta k)$, i.e. no harmonic power is emitted below threshold (see Eq. (34)). From the above-threshold expression Eq. (33) we see that the onset of parametric oscillation can cause the external SHG efficiency to turn on, as $C(\Delta K, \Delta k) I(\Delta K)$ typically is nonzero. This effect is possible since the circulating signal and idler waves generate the sum frequency $2\omega_1$ with a gain $I(\Delta K)$ which is large when $\Delta KL \approx 0$. In Fig. 7 we compare the efficiency of SPO-induced SHG at a zero of the usual SHG ($\Delta kL = 21\pi$) with the usual SHG efficiency, given by

$$\frac{P_{2,\mathrm{out}}}{P_{1,\mathrm{in}}} = \frac{\left(\sqrt{1+\tilde{p}} - 1\right)^2}{\tilde{p}}, \quad \tilde{p} = |I(\Delta k)|^2 \frac{P_{1,\mathrm{in}}}{\bar{P}(T=0)}, \tag{36}$$

at a phasematching peak nearby ($\Delta kL = 20\pi$), assuming SPO to be quenched. The efficiencies are quite similar; this indicates that in the case of large phase mismatch SPO does not prevent the harmonic generator from reaching conversion efficiencies on the order of 10% for input powers at the 10 W level.

4. Quantum fluctuations

The quantum properties of the SPO may be derived using well-established techniques. These consist in translating the classical equations of motion of the fields to the quantum analog, linearizing the resulting equations for small fluctuations of the fields around the classical steady-state solutions, and obtaining an input-output matrix relating the fluctuations of the waves injected into the nonlinear system to the fluctuations of the waves leaving it. The quantum noises can then be calculated from the matrix elements. As it is essential to consider all sources of input quantum noise, Eqs. (22) must be extended to include input harmonic and signal/idler waves. To keep the discussion simple, we shall take the special case of zero phase mismatches, weak focusing, and zero detunings. We obtain the equations of motion

$$\dot{\alpha}_1 = -\gamma\alpha_1 - \frac{\mu}{2}|\alpha_1|^2\alpha_1 - \sqrt{\mu\nu}\,\alpha_i\alpha_s\alpha_1^* - \sqrt{\mu}\,\alpha_1^*\alpha_{2,\mathrm{in}} + \sqrt{2\gamma_c}\,\alpha_{1,\mathrm{in}},$$

$$\dot{\alpha}_{i/s} = -\gamma\alpha_{i/s} - \nu|\alpha_{s/i}|^2\alpha_{i/s} - \frac{\sqrt{\mu\nu}}{2}\alpha_1^2\alpha_{s/i}^* - \sqrt{\nu}\,\alpha_{s/i}^*\alpha_{2,\mathrm{in}} + \sqrt{2\gamma_c}\,\alpha_{i/s,\mathrm{in}}. \tag{37}$$

where we have introduced the harmonic, idler and signal input fields $\alpha_{2,\mathrm{in}}$, $\alpha_{i/s,\mathrm{in}}$. The last two relations in Eqs. (23) are also generalized,

$$\alpha_{i/s,\mathrm{out}} + \alpha_{i/s,\mathrm{in}} = \sqrt{2\gamma_c}\,\alpha_{i/s}, \qquad \alpha_{2,\mathrm{out}} = \alpha_{2,\mathrm{in}} + \sqrt{\mu}\,\alpha_1^2 + 2\sqrt{\nu}\,\alpha_i\alpha_s. \tag{38}$$

The nonlinear system described by Eqs. (37) and (38) encompasses as special cases important systems that have been studied in the past both theoretically and experimentally: for $\nu = 0$ (no parametric interaction) and no harmonic input mean field,

$\alpha_{2,\mathrm{in}} = 0$ we recover the singly-resonant frequency doubler [5]. For $\mu = 0$ (no SHG interaction) and no idler/signal input mean field, $\alpha_{\mathrm{i/s,in}} = 0$ we have the nondegenerate parametric oscillator. To facilitate comparison with the literature, we now consider the plane-wave case; to this end the harmonic field and the nonlinear couplings are rescaled as $\alpha_{2,\mathrm{in/out}} \to \sqrt{2}\ \tilde{\alpha}_{2,\mathrm{in/out}}$, $\mu \to 2\tilde{\mu}$, $\nu \to 2\tilde{\nu}$.

Below SPO threshold

It is easy to show that below threshold, where $\alpha_{\mathrm{s/i}} = 0$, the linearized equation of motion of the subharmonic and harmonic fluctuation operators are identical to those of usual singly-resonant SHG [5]. The presence of parametric gain for subthreshold signal/idler waves does not lead to consequences for subharmonic and harmonic since the signal and idler mean fields are zero. The amplitude quantum noise variances of harmonic and subharmonic are minimum at zero frequency and decrease to 1/2 and 3/4 of the coherent state level, respectively, just below threshold [5].

In order to discuss the signal/idler noise below threshold, we note an important analogy. The nondegenerate OPO is formally similar to the SPO: as Eqs. (37) show, the driving force for signal and idler is the externally injected harmonic wave $2\alpha_{2,\mathrm{in}}$ in the first case, and the subharmonic circulating power $\sqrt{\tilde{\nu}}\alpha_1^2$ in the second. Note however that the latter is a positive definite quantity, in contrast to $\alpha_{2,\mathrm{in}}$. This analogy extends to the quantum behavior: in both cases the input quantum noises of the subharmonic (and the vacuum noise of the harmonic) do not couple to the signal/idler fields below threshold. As for the nondegenerate OPO, the SPO generates twin beams. We omit explicit expressions for the quantum noises, since they have been extensively discussed [26]. The only change therein is the replacement of the normalized pump power $P_{2,\mathrm{in}}/P_{\mathrm{DRO}} = 4\tilde{\nu}\tilde{\alpha}_{2,\mathrm{in}}^2/\gamma^2$ by the square of the ratio of circulating subharmonic power relative to its value at SPO threshold, $\tilde{\nu}^2\alpha^4/\gamma^2$. The important final result is that at SPO threshold and zero frequency, the variance in the difference of signal and idler fields reaches $1 - \gamma_c/\gamma$, and thus a high degree of correlation is obtained for a cavity with large escape efficiency.

Above SPO threshold

To obtain the above-threshold quantum properties of the SPO, we can make use of the results derived by Marte for parametric oscillation in doubly-resonant SHG [23,25]. In the latter system, the harmonic wave is resonant, and obeys an additional equation of motion. If the decay of the harmonic wave (decay rate γ_2) is much faster than any other dynamics, the harmonic wave can be adiabatically eliminated. The resulting three equations of motion for the subharmonic, signal/idler waves as well as the algebraic equation for the output harmonic wave are then formally identical to the plane wave-form of Eqs. (37) and (38). The correspondence is obtained by setting in those equations

$$\tilde{\mu} \to \frac{\kappa^2}{2\gamma_2}, \quad \tilde{\nu} \to \frac{\chi^2}{2\gamma_2}, \tag{39}$$

where κ and χ are the coupling constants of Ref. [25]. As a consequence of this correspondence, the quantum noises for singly-resonant SPO are obtained from those for harmonic-resonant SPO by letting $\gamma_2 \to \infty$ in the latter. In the spirit of simplicity we consider equal coupling strengths, $\kappa = \chi$ (i.e. $\mu = \nu$) and unity escape efficiencies ($\gamma = \gamma_c$). From Eqs. (6)–(9) of Ref. [25], setting $s = 1$, $r = 1$, we obtain the normalized quantum noise powers of amplitude (a) and phase (b) quadrature fluctuations,

$$V_{a1}(\hat{\Omega}) = 1 - \frac{1 - \epsilon + \hat{\Omega}^2}{4\epsilon^2\hat{\Omega}^2 + (-1 + \epsilon - \hat{\Omega}^2)^2}, \qquad V_{b1}(\hat{\Omega}) = 1 + \frac{\epsilon + \hat{\Omega}^2}{4\epsilon^2\hat{\Omega}^2 + (\epsilon - \hat{\Omega}^2)^2}, \tag{40}$$

$$V_{a2}(\hat{\Omega}) = 1 + \frac{2(-1 + \epsilon - \hat{\Omega}^2)}{4\epsilon^2\hat{\Omega}^2 + (-1 + \epsilon - \hat{\Omega}^2)^2}, \qquad V_{b2}(\hat{\Omega}) = 1 + \frac{2(\epsilon + \hat{\Omega}^2)}{4\epsilon^2\hat{\Omega}^2 + (\epsilon - \hat{\Omega}^2)^2}, \tag{41}$$

where $\hat{\Omega} = \Omega/2\gamma$, $\epsilon = P_{1,\mathrm{in}}/P_{1,\mathrm{in}}^{\mathrm{th}} > 1$ and $P_{1,\mathrm{in}}^{\mathrm{th}} = 4\bar{P}$ is the SPO threshold at $\Delta kL = \Delta KL = 0$.

We are now in a position to discuss the above-threshold behavior of the intensity (amplitude) quantum noise of the fundamental and harmonic waves. As noted by Marte, above threshold the harmonic amplitude noise is always above shot noise for zero frequency, with a divergence at threshold due to the diverging quantum noise of signal and idler. The minimum amplitude noise occurs at a nonzero frequency Ω_{opt}, given for both the subharmonic and the harmonic waves by

$$(\Omega_{\mathrm{opt}}/2\gamma)^2 = \epsilon - 1 + \epsilon\sqrt{\epsilon - 1}\,. \tag{42}$$

This optimum frequency grows monotonically from zero as the SPO is driven further above threshold. The minimum noise levels are

$$V_{a1}(\Omega_{\rm opt}) = 1 - \frac{1}{2\epsilon(\epsilon + \sqrt{\epsilon - 1})}, \qquad V_{a2}(\Omega_{\rm opt}) = 1 - \frac{1}{4\epsilon(\epsilon + \sqrt{\epsilon - 1})}. \tag{43}$$

At threshold, these expressions connect without discontinuity to the values just below threshold cited above. The important result contained in Eq. (43) is that the minimum quantum noise above threshold increases monotonically with input power and is larger than the value achievable below threshold. This result indicates the importance of preventing SPO when operating singly-resonant frequency doublers as sources of bright squeezed light. Tsuchida [7] reported 5.2 dB of quantum noise reduction in singly-resonant SHG. Such a value appears to imply that SPO did not occur in his system.

The correlations between the signal and idler beams above threshold are described by the intensity sum and difference quantum noise powers,

$$V_{\rm sum}(\hat{\Omega}) = 1 + \frac{1 + 3\epsilon + \hat{\Omega}^2}{4\epsilon^2\hat{\Omega}^2 + (-1 + \epsilon - \hat{\Omega}^2)^2}, \qquad V_{\rm diff}(\hat{\Omega}) = 1 - \frac{1}{1 + \hat{\Omega}^2}. \tag{44}$$

$V_{\rm sum}$ is always above the shot noise level. The result for the intensity difference $V_{\rm diff}$ is particularly simple and identical to those for the harmonic-resonant SPO [25] and the conventional DRO [27]. It is independent of the subharmonic pump power. In the presence of cavity loss, the zero frequency value of zero is replaced by $1 - \gamma_c/\gamma$. Twin beams with strong correlations are thus expected above the SPO threshold if the escape efficiency is high. On the other hand, each individual beam can reach a maximum amplitude noise suppression of 3 dB, at zero frequency and far above threshold.

5. Conclusion

We have analyzed some of the properties of the subharmonic-pumped parametric oscillator and put them in context with usual singly-resonant SHG and cascaded $\chi^{(2)}$ effects in a cavity. The main goal of the analysis was to study how the SPO threshold and the conversion efficiency depend on experimentally controllable parameters. Arbitrary wavevector mismatches for the two individual conversion processes, the second-harmonic generation and the parametric generation, were therefore taken into account. The former is controlled by the temperature or orientation of the nonlinear crystal. The parametric wavevector mismatch will typically be the one that minimizes the threshold. Our calculation yields the Δk-dependence of the SPO threshold, so that the preferred oscillation wavelengths can be determined. We emphasize, however, that for a precise prediction of the output spectrum for given Δk, the discrete mode spectrum of signal and idler (giving rise to a clustering effect [9]) and possible spectral characteristics of the cavity mirrors must also be considered.

The threshold and conversion efficiency of the SPO exhibit distinct behaviours depending on the phase mismatches. While at $\Delta k = \Delta K = 0$ optical limiting in the harmonic and constant slope efficiency for signal/idler generation are found, at other mismatches the conversion efficiency is nonmonotonic. Near $\Delta k = \Delta K = 0$ we find a relatively complicated dependence of the threshold on the mismatches. The minimum threshold is found to be almost a factor two lower than that at $\Delta k = \Delta K = 0$.

Two central consequences of the fact that the harmonic amplitude over the whole nonlinear medium contributes to the gain for signal and idler are that

(i) SPO can occur even when Δk is such that the net second-harmonic generation efficiency is zero. Once parametric generation sets in, there is generation of the second harmonic wave, but through the sum-frequency process;

(ii) For large $|\Delta k|$ the SPO threshold increases linearly with $|\Delta k|$ within the Δk-intervals where the threshold is lowest.

The conversion efficiency for subharmonic input to signal plus idler is relevant for application of the SPO as a frequency converter. Values in the range of tens of percent can be reached for input powers a few times above threshold. This is in agreement with recent experiments [10] and shows that the SPO has potential as an efficient frequency converter.

It should be noted that stable multi-mode oscillation of the SPO was observed already in the first implementation of the SPO [8,9]. This effect deserves a detailed theoretical analysis since it may lead to limits in the conversion efficiency of SPO.

Regarding the quantum properties of the SPO we find that on one hand the degree of squeezing in the harmonic wave is reduced above threshold due to coupling to the quantum noise of the signal and idler waves. Therefore, if a singly-resonant frequency doubler is to be used to generate substantially squeezed light (> 3 dB), it must be designed to avoid SPO, e.g. using intracavity etalons. On the other hand, the quantum correlation between signal and idler waves can be excellent both below and above threshold, just as for the usual parametric oscillator. In applications where near-degenerate signal/idler twin beams are desired and the pump wave for the oscillator has first to be generated by SHG, the SPO may represent a replacement for separate resonant SHG and OPO devices.

Acknowledgements

We thank Prof. J. Mlynek for supporting this work. We are indebted to R. Paschotta, G. Breitenbach and K. Schneider for many stimulating discussions and their contributions to this research program. M.A.M. Marte kindly provided the expressions (40), (41), (44). This work was performed as part of ESPRIT LTR Project 6934 QUINTEC. Additional support was provided by the Optik-Zentrum Konstanz.

References

[1] A. Ashkin, G.D. Boyd and J.M. Dziedzic, J. Quantum Electron. QE-2 (1966) 109.
[2] Z.Y. Ou, S.F. Pereira, E.S. Polzik and H.J. Kimble, Optics Lett. 17 (1992) 640.
[3] R. Paschotta, K. Fiedler, P. Kürz, R. Henking, S. Schiller and J. Mlynek, Optics Lett. 19 (1994) 1325.
[4] K. Schneider, S. Schiller, J. Mlynek, M. Bode and I. Freitag, Optics Lett. 21 (1996) 1999.
[5] R. Paschotta, M. Collett, P. Kürz, K. Fiedler, H.-A. Bachor and J. Mlynek, Phys. Rev. Lett. 72 (1994) 3807.
[6] T.C. Ralph, M.S. Taubman, A.G. White, D.E. McClelland and H.-A. Bachor, Optics Lett. 20 (1995) 1316.
[7] H. Tsuchida, Optics Lett. 20 (1995) 2240.
[8] S. Schiller, G. Breitenbach, S.F. Pereira, R. Paschotta, A.G. White and J. Mlynek, Proc. SPIE, Vol. 2378, ed. Y. Shevy (1995) p. 91.
[9] S. Schiller, G. Breitenbach, R. Paschotta and J. Mlynek, Appl. Phys. Lett. 68 (1996) 3374.
[10] K. Schneider and S. Schiller, Optics Lett., in press.
[11] A.G. White, P.K. Lam, M.S. Taubman, M.A.M. Marte, S. Schiller, D.E. McClelland and H.-A. Bachor, Classical and quantum signatures of competing $\chi^{(2)}$ nonlinearities, submitted.
[12] S. Schiller and R.L. Byer, J. Opt. Soc. Am. 10 (1993) 1696.
[13] See references in: G. Assanto, G.I. Stegeman, M. Sheik-Bahae and E. VanStryland, J. Quantum Electron. 31 (1995) 673.
[14] A.G. White, J. Mlynek and S. Schiller, Europhys. Lett. 35 (1996) 425.
[15] J. Sorensen, E. Polzik and J. Ostergaard, poster, Les Houches School, Second-order nonlinear optics: from fundamentals to applications, April, 1996.
[16] G.D. Boyd and D.A. Kleinman, J. Appl. Phys. 39 (1968) 3597.
[17] S. Guha, F.-J. Wu and J. Falk, J. Quantum Electron. QE-18 (1982) 907; R. Fischer, P.V. Nickles, T.R. Chu and L.-W. Wieczorek, Ann. der Physik 39 (1982) 287; T.-B.-Chu and M. Broyer, J. de Physique 45 (1984) 1599.
[18] A.E. Siegman, Lasers (University Science Books, 1986).
[19] G. Breitenbach, S. Schiller and J. Mlynek, J. Opt. Soc. Am. 12 (1995) 2095.
[20] L.A. Lugiato, C. Oldano, C. Fabre, E. Giacobino and R.J. Horowicz, Nuovo Cimento 10 D (1988) 959.
[21] P. Drummond, K.J. McNeil and D.F. Walls, Optica Acta 27 (1980) 321.
[22] G. Breitenbach, S. Schiller and J. Mlynek, J. Opt. Soc. Am. 12 (1995) 2097.
[23] M.A.M. Marte, Phys. Rev. A 49 (1994) R3166.
[24] A.E. Siegman, Appl. Optics 1 (1962) 739.
[25] M.A.M. Marte, Phys. Rev. Lett. 74 (1995) 4815.
[26] S. Reynaud, C. Fabre and E. Giacobino, J. Opt. Soc. Am. 4 (1987) 1520; Z.Y. Ou, S.F. Pereira and H.J. Kimble, Appl. Phys. B 55 (1992) 265.
[27] J. Mertz, T. Debuisschert, A. Heidmann, C. Fabre and E. Giacobino, Optics Lett. 16 (1991) 1234.